The Effects of Surface Roughness and Metal Temperature on the Heat-Transfer Coefficient at the Metal Mold Interface

BASIL COATES and STAVROS A. ARGYROPOULOS

This article focused on the effects of surface roughness and temperature on the heat-transfer coefficient at the metal mold interface. The experimental work was carried out in a unique and versatile apparatus, which was instrumented with two types of sensors, thermocouples, and linear variable differential transformers (LVDTs). The monitoring of the two types of sensors was carried out simultaneously during solidification. The concurrent use of two independent sensors provided mutually supportive data, thereby strengthening the validity of the interpretations that were made. With this type of instrumentation, it was possible to measure temperature profiles in mold and casting, as well as the air gap at the metal mold interface. Commercial purity aluminum was cast against steel and high carbon iron molds. Each type of mold had a unique surface roughness value. Inverse heat-transfer analysis was used to estimate the heat-transfer coefficient and the heat flux at the metal mold interface. A significant drop in the heat-transfer coefficient was registered, which coincided with the time period of the air gap formation, detected by the LVDT. An equation of the form $h = \frac{1}{b^* A + c} + d$ was found to provide excellent correlation between the heat-transfer coefficient and air gap size. In general, an increase in mold surface roughness results in a decrease in the heat-transfer coefficient at the metal mold interface. On the other hand, a rise in liquid metal temperature results in a higher heat-transfer coefficient.

I. INTRODUCTION

THE heat-transfer coefficient at the metal mold interface plays a very important role in predicting the solidification rate and grain structure of a metal. In solidification modeling, the heat-transfer coefficient represents an important input parameter. The accuracy of this input parameter affects the accuracy of the solidification modeling predictions. Many factors affect the value of a heat-transfer coefficient at the metal mold interface, and there is a need to investigate, and if possible, to quantify these factors.[1,2]

Sully[3] reported that during casting solidification, heat flow reaches a maximum within a few seconds and then falls, sometimes at continuously changing rates. The latter is reportedly associated with the separation of the casting surface from the mold surface. This physical separation results in the formation of an air gap, which incidentally reduces the heat-transfer rate.[4–8] The mechanism governing heat transfer between a solidifying liquid metal against a metal mold/chill has been the subject of intense investigation by Ho and Pehlke[9,10] and Pehlke.[11] They suggested that heat transfer is initiated by conduction: (1) through contact between a thin solidified skin and the peaks of the rough surface and (2) through the gas contained in the voids between the contact areas. Further, as solidification progresses, relative thermal expansion and contraction of the chill and casting can result in a reduction in the contact areas resulting in an increase in void. Eventually this leads to a complete separation and the formation of an air gap. The formation of an air gap has a dramatic effect on the reduction of heat-transfer coefficient values. The value of the heat-transfer coefficient can be influenced further by several factors, including the presence and thickness of surface coatings,[12–15] casting surface orientation,[16,9,17] casting size,[15,16,18] mold material,[8,16,9] liquid alloy surface tension,[19] mold preheat,[20,21] alloy superheat,[8,22,23] and chill surface roughness.[2,8,12,23–26]

The fundamentals of the casting process dictate that some amount of superheat must be applied in order to effectively fill any mold cavity. The effects of superheat on heat-transfer coefficient values have been investigated extensively by numerous scientists.[8,18,22] Muojekwu et al.[8] conducted experiments with Al-Si alloys cast against water-cooled chills made from copper, brass, steel, and cast iron. The results presented showed that interfacial heat flux and heat-transfer coefficients increased with increased superheat. The increase in heat flow was attributed to an increase in interfacial contact, which can be traced to two influencing phenomena. The first case can be represented by an increase in the fluidity of the aluminum alloy,[25] which enhances the likelihood of the liquid metal filling more mold surface cavities. Second, higher superheat does not support the early formation of a thick rigid shell, which would otherwise

---

BASIL COATES, Formerly Graduate Student, Department of Material Science and Engineering, University of Toronto, is with the Hentel Litecare Corporation, Brooklyn, NY 11224. STAVROS A. ARGYROPOULOS, Professor, is with the Department of Material Science and Engineering, University of Toronto, Toronto, ON, Canada M5S 3E4. Contact e-mail: stavros.argyropoulos@utoronto.ca

pull away from the chill and create an air gap. Furthermore, any retardation in the formation of a shell would render a greater initial driving force ($T_C - T_m$) for heat flow across the interface. Taha *et al.*[18] conducted similar experiments, casting Al and Al-Cu alloys against sand and copper end molds. The results of heat-transfer coefficient values, though varied in trend for the two chills, increased with increased superheat. El-Mahallaway *et al.*[22] conducted similar experiments involving liquid aluminum solidifying against a copper mold. The results presented showed that 115 K super-heat yielded 3 times higher heat-transfer coefficient values, over the 40 K superheat.

Heat-transfer coefficient values are also affected by mold surface roughness.[8,9,23,24] Muojekwu *et al.*[8] studied the relationship between heat transfer and microstructure evolution of secondary dendrite arm spacing and incorporated, among other variables, the effects of surface roughness. Results revealed that heat-transfer coefficient values were higher for smoother surfaces. They observed that a 16-fold increase in the value of roughness from 0.018 to 0.29 μm resulted in a 12.5 pct decrease in heat flux and a 17.0 pct decrease in heat-transfer coefficient values. Again, it was noted that if the value of surface roughness was increased to more than 500-fold to 10.56 μm, the heat flux decreased by about 32.0 pct while the heat-transfer coefficient decreased by about 41.0 pct. Schmidt *et al.*[12] conducted experiments involving several mold surface conditions. The results showed that when a mold was polished, the maximum heat-transfer coefficient increased by a factor of 2. Chiesa[23] also conducted experiments to measure thermal conductance at the metal mold interface. These experiments involved casting A356 aluminum alloy against cast iron molds. Surface coating applied to the mold surface created surface roughness values varying from 1.0 to 25 μm. The results presented showed that the coating providing higher surface roughness values resulted in lower heat-transfer values. Assar[24] conducted similar experiments involving pure zinc and a vertically oriented cylindrical core mold. Information on radial heat flow for three surface roughness values, 0.043, 0.173, and 0.303 μm, was gathered. The results showed that heat-transfer coefficient values increased with the decrease in surface roughness values.

The dynamic behavior of the interfacial heat transfer between a solidifying molten metal and a substrate also have been investigated by many authors using low melting point metals such as tin, lead, and zinc.[27–30]

Whereas previous work has determined that there is an inverse relationship between the magnitude of the air gap and that of the heat-transfer coefficient, little is known about the precise relationship of the two. The limited number of techniques that have attempted to measure the air gap and the heat-transfer coefficient attests to the complexity of the issue. Initially, the concept of electrical capacitance in cylindrical condensers was used to measure the air gap.[31] However, as the authors acknowledged, this method is limited by the fact that only an average air-gap between the cast and the mold can be determined; the more important individual movements of cast and mold cannot be detected directly. Moreover, the accuracy of this technique depends on the geometry of the mold. Other investigators used an estimate of the propagation of an ultrasonic signal through a casting-chill interface to infer the degree of actual contact occurring between cast and mold.[32] But this technique is handicapped by the fact that it can only provide information for the first 2 seconds of casting.

The forgoing discussion indicates that it would be meritorious to develop a methodology capable of overcoming the limitations of the techniques used in the past. As such, the main aim of this research was to develop a technique capable of (a) determining the magnitude of the heat-transfer coefficient over time and (b) concurrently measuring the onset of the formation of the air gap and tracking its magnitude over time. Once this is achieved, it will be possible to develop a mathematical equation describing the relationship between heat-transfer coefficient and air gap size. A secondary aim was to analyze the effects of various parameters such as mold roughness and metal temperature on the heat-transfer coefficient.

This research work was carried out in a specially built apparatus, instrumented with thermocouples and displacement sensors (linear variable differential transformer (LVDT)). The results of heat-transfer coefficient values to be shown herein were obtained through the development of a computer code, which follows an algorithm based on the well-known nonlinear inverse heat conduction problem.[33] The heat-transfer coefficient was estimated at each 1-second interval, beginning from the time of pouring to 2500 seconds after pouring.

II. EXPERIMENTAL

A. *Description of Experimental Apparatus*

The mold assembly, Figure 1, is a novel two-tier (vertical and horizontal) offset T-shaped steel case unit, mounted on a trapezoid shaped space frame. The inside of this unit is lined with 38-mm-thick alumina-silicate fiber refractory insulation to ensure that a one-dimensional heat flux from the casting to the mold can be created along the longitudinal direction. The vertically oriented cylindrical section was designed in two halves (*i.e.*, split) to allow for easy removal of the predominantly L-shaped casting that was produced. This section houses a 127-mm o.d. × 50-mm i.d. fiber refractory form. The design allows it to be used as a riser, with a pouring basin at the bottom to capture the initial inertia of the down pouring molten stream, so as to reduce streaming velocity. It carries two bleed holes near the upper open end. These holes can be unplugged to provide some measure of automatic control of a desired metallostatic pressure head during solidification. This vertical section is joined at its lower end by a smaller (101-mm) horizontal cylindrical section. Unlike the vertical section, it houses a 25-mm-thick monotype constructed insulating form with a 50- to 54-mm tapered inner casting core. The outer end of this cylinder carries two 25-mm-thick high-density refractory board discs. One disc (25-mm thick × 50-mm i.d.) is fully contained within
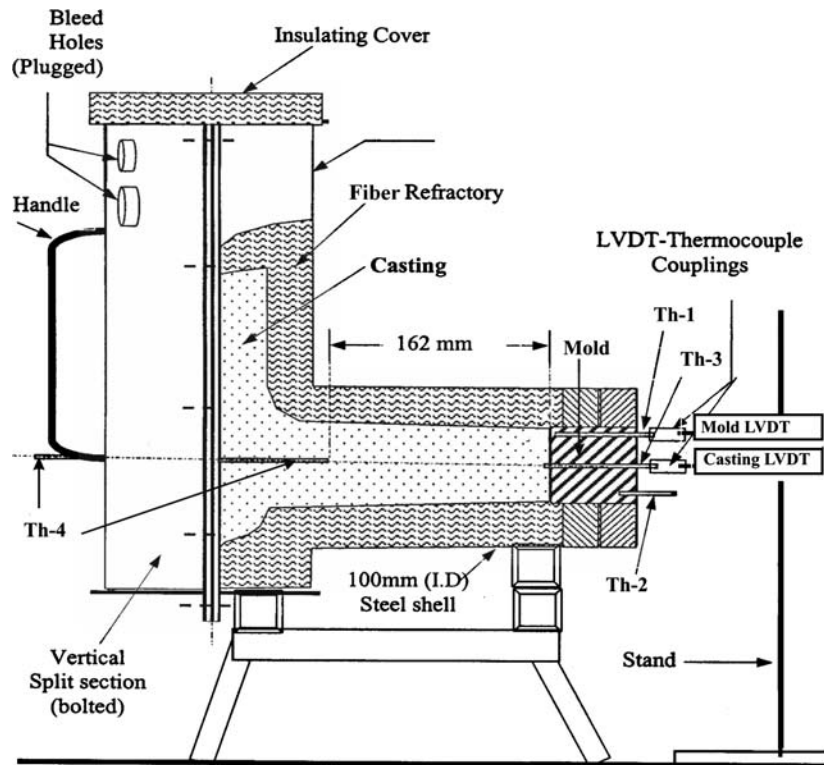
Fig. 1—Schematic cross section of the apparatus developed.

the steel shell, while the other, a stepped disc, is partially contained with part of it slightly overlapping the steel shell diameter. The outer stepped disc provides an additional 25-mm support for the mold and aids in securing the entire mold end.

This investigation focused on the horizontal casting configuration, as illustrated in Figure 1. Casting orientation can be described according to two common axes, vertical and horizontal. In the vertical plane, there are two possible configurations: one with the casting on top of the mold and the other with the mold on top of the casting. These orientations lead to various physical phenomena and distinct regimes of heat-transfer coefficient values.[2,14] This study, by comparison, deals with the middle regime of the heat-transfer coefficient values. It was observed that the casting in the horizontal casting configuration, coupled with the type of mold fiber refractory lining, could suffer some restriction in contraction due to the spongy nature of the refractory lining. To cancel this effect, the mold "well" was designed to create an anchor when the liquid metal solidified at the base. This provided for a single directional contraction of the casting away from the chill surface. Figure 2 displays details of the mold "well."

Two DC operated LVDT, made by H.A. Schaevitz (U.S.A.), type DC-750-125-0006 and DC-E250, were used to simultaneously measure movement in the mold (correspondingly associated with expansion) and
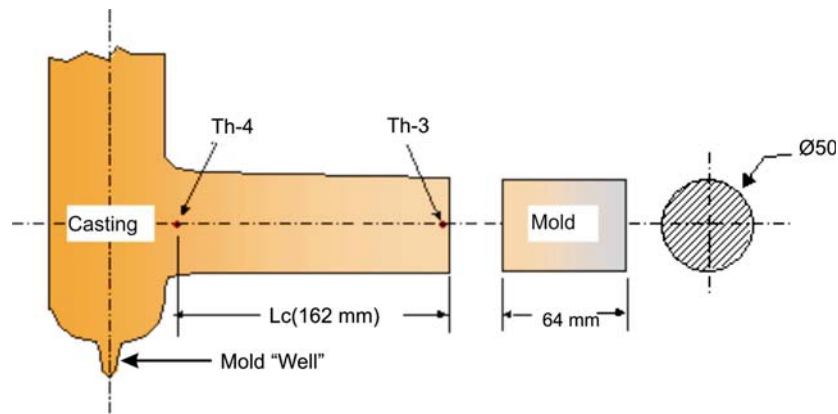

Fig. 2—Details of the mold "well".

movement in the casting (correspondingly associated with contraction). Type DC-750-125-0006 with a nominal range of 6.0 mm was used to monitor the mold's expansion movement and it is labeled LVDT-1. This LVDT with the higher resolution was deliberately selected for the mold owing to its relatively smaller expected expansion, as compared to the anticipated contraction in the casting. The casting LVDT had a nominal range of 12.0 mm and it is labeled LVDT-2. The center of each mold was drilled through to accommodate a 3- to 4 mm-diameter quartz rod coupled to the LVDT-2. The LVDT-2 was used to monitor the movement in the casting. The difference between the displacement measurements of LVDT-1 and LVDT-2 indicates the relative movement of the mold-casting metal interface. Throughout this research work, temperature measurements were carried out using *K* type of thermocouples. The calibration of these thermocouples was performed by measuring the solidification temperature of commercial purity aluminum. The small difference between the expected (660 °C) and observed (661.1 °C) temperature at the solidification plateau indicated the accuracy of temperature measurements. Figure 1 shows the positions of various thermocouples used. Th-1 and Th-2 are the thermocouples, which are located in the mold. Their exact position is shown in Figure 3. Th-3 and Th-4 are sacrificial thermocouples located in the casting and can be seen in Figure 1. Both LVDTs were coupled with the thermocouples. The pairing was set in such a manner that the mold LVDT-1 was coupled with Th-1, while the casting LVDT-2 was coupled with Th-3. A data acquisition system (μMac-6000) was used. This data acquisition system is programmable *via* μMac-Basic programming language and has a 14-bit resolution, A/D converter. The melting of the castable metal was done with the aid of a Bradley coreless induction furnace (Ontario, CANADA).

B. *Experimental Procedure*

The main consumable material in this research work was commercially pure aluminum as the casting metal against two different molds. The first type of mold was 1020 steel (hypoeutectoid steel), and the second type of mold was cast iron. Table I shows several thermal and physical properties relating to these materials.

1. *Mold surface roughness preparation*
Figure 3 shows the metal mold details and dimensions. As seen in this figure, one side of the mold had special
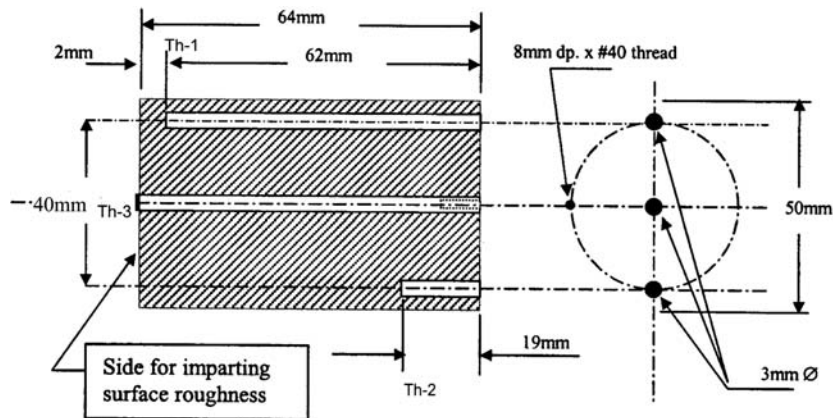

Fig. 3—Horizontal cross-sectional view of the metal mold.

Table I.   Physical Properties of Steel Chill and Commercially Pure Aluminum

Chill Material	Density (kg m^{-3})	Thermal Conductivity (W m^{-1}K^{-1})	Specific Heat Capacity (J kg^{-1}K^{-1})	Chemical Composition on Major Elements in wt pct
Steel (1020)	7870	52	486	C: 0.17 to 0.23 Fe: 99.08 to 99.53 Mn: 0.3 to 0.6 P: max 0.04 S: max 0.05
High carbon iron	7100	36	515	C: 3.0 to 4.0 Si: 1.8 to 2.8 Mn: 0.10 to 1.00 S: max 0.03 P: max 0.10
Aluminum (commercial purity)	2700	95.4 (liquid) 213 (solid)	1080 1080	—

surface roughness, which was imparted using a lathe. Surface profiles were deliberately imparted and varied from plain to *v* groove in shape so as to study the effect of surface roughness. The information gathered and plotted produced a relationship between surface roughness values and machine lathe settings. The established relationship provided guidance in prescribing several distinct operations to produce a range of surface roughness values to span the industrial application spectrum.[34] The surface of each mold specimen was then evaluated for its specific surface roughness (R_a) value using a special stylus surfometer. In this research work, three surfaces with roughness values R_a = 1.41, 20.72, and 32.69 μm form part of the list of test parameters.

2. *Casting procedure*

In order to adequately realize sound casting and accurate data collection, the following procedure was executed for each experiment.

(1) The mold (64 mm × 50 mm diameter), seen in Figure 3, was inserted at the horizontal opening of the assembly. With the aid of fixing pins for alignment, the mold was positioned such that the two thermocouple holes on the outer periphery lay on the same horizontal axis. Next, with the retainer disc and bar in place, the chill position along the horizontal axis was set by manipulating the centrally located hollow set screw.

(2) Two spring-loaded thermocouples were inserted into the chill, one at 2 mm from the interface and the other closer to the end of the chill, to record temperature changes while maintaining firm contact.

(3) In addition to recording temperature at 2 mm behind the steel mold's interface, a unique technique was implemented to monitor simultaneously any movement of the interface by coupling the thermocouple to the LVDT-1.

(4) On the casting side, a similar novel technique was implemented. In this case, a thermocouple with a groove approximately 2 mm from the thermocouple end was attached to the LVDT-2. An anchor twist, made from approximately AWG 36 gage wire, was wrapped around the groove. The wire ends of this anchor were fixed so that they projected into the casting side. Once assembled the thermocouple wire end was made to project 2 mm beyond the steel mold interface boundary and into the casting metal. This arrangement ensured that data on temperature and air gap development were collected simultaneously.

(5) All sensors were linked to the PC computer *via* the μMac-6000 data acquisition system. This system was activated to collect data just before pouring.

(6) The entire assembly was located within close proximity to the induction furnace.

(7) The aluminum casting metal was placed in a red-clay covered clay graphite crucible, which provided greater control in cooling. The batch of metal was then heated in the induction furnace to a temperature about 20 °C above the required

pouring temperature. The crucible was moved from the furnace, and the slag and dross from the melt skimmed. During this time, the melt was allowed to cool to the pouring temperature (either 680 °C or 760 °C).

(8) When the desired temperature was reached, the induction furnace was turned off in order to minimize any electrical interference between furnace and the data acquisition apparatus/system.

(9) The data acquisition system was activated to record temperature and displacement readings for a time period of 2500 seconds.

(10) Next, the assembly was filled with liquid metal within 3 seconds, and the riser end was covered with the same insulating material as the assembly.

(11) Step 10 was repeated for all casting operations.

(12) Finally, the data collected were analyzed using an inverse heat-transfer procedure.

III. ESTIMATION OF HEAT FLUX AND HEAT-TRANSFER COEFFICIENT USING AN INVERSE HEAT-TRANSFER PROCEDURE

A. *Problem Formulation*

This experiment employed a unique versatile apparatus along with the use of different thermocouples at various locations in the cylindrical refractory fiber. This experimental setup afforded the opportunity to establish that the heat transfer through the mold is essentially a one-dimensional heat transfer. The estimation of the heat flux was based on solving inversely the one-dimensional transient heat conduction equation, following the procedure suggested by Beck.[33] The following equation describes the one-dimensional transient heat conduction equation:

$$\frac{\partial T}{\partial t} = \alpha \frac{\partial^2 T}{\partial x^2} \qquad [1]$$

where $a = \frac{k}{\rho C_p}$, T is temperature, t is time, C_p is specific heat, k is thermal conductivity, x is distance, and ρ is density subject to the following initial and boundary conditions:

$$T(x, 0) = T_i(x) \qquad [2a]$$

$$-k \frac{\partial T}{\partial x} = q(0, t) \qquad [2b]$$

$$T(x_1, t) = Y_1(t) \qquad [2c]$$

$$T(x_2, t) = Y_2(t) \qquad [2d]$$

where

T_i = initial uniform temperature of mold;
q = heat flux at the casting mold interface;

x_I, x_2 = mold thermocouples' distance from the mold surface, 2 and 45 mm, respectively; and

Y_1, Y_2 = temperature measured by mold thermocouples and used as boundary conditions in the mold, illustrated in Figure 4(a).

Equation [1] was solved using the explicit finite difference method. In Figure 4(b), the suffix i represents the exterior node, J the interior nodes, and O the measured boundary condition. The following finite difference equation was used to calculate the interior node J at time-step $t + 1$:

$$T_J^{t+1} = \frac{\alpha \Delta t}{(\Delta x)^2} \left(T_{J+1}^t + T_{J-1}^t\right) + T_J^t \left(1 - 2\alpha \frac{\Delta t}{(\Delta x)^2}\right)$$

[2e]

and for exterior node i at time-step $t + 1$, T_i^{t+1} is given by

$$T_i^{t+1} = T_i^t - \frac{2\alpha\Delta t}{(\Delta x)^2}\left(T_i^t - T_{i-1}^t\right) + \frac{2q\Delta t}{(\rho\, C_p \Delta x)} \quad [2f]$$

In Eq. [2f], node $i - 1$ corresponds to the next of i node in the mold, as seen in Figure 4(b). In the preceding finite difference equations, the α represents the thermal diffusivity of the mold. The Fourier number, Fo, is given as Fo $= \frac{\alpha \Delta t}{(\Delta x)^2}$. The Δx was selected to be 1.0 mm and the value of Δt was chosen to satisfy the stability criterion Fo ≤ 0.5.

In the solution, boundary conditions $q(0,t)$ and $T(0,t)$ were estimated simultaneously by minimizing the following function given in Eq. [3]:

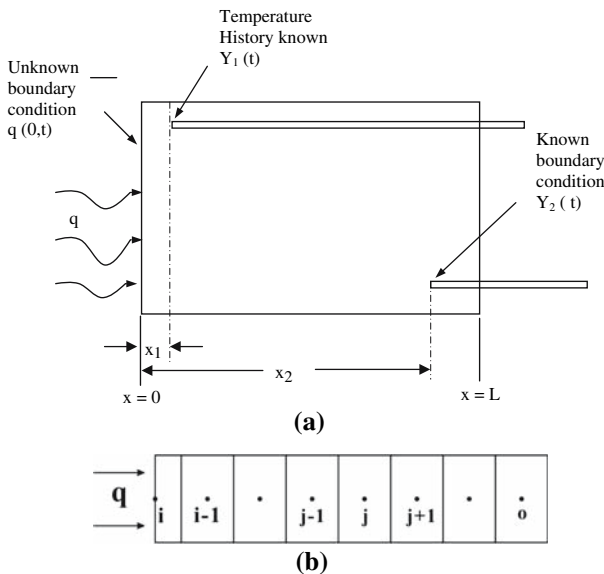$$F(\overline{q}\,) = \sum_{i=1}^{I} (T_{n+i} - Y_{n+i})^2 \quad [3]$$

where I is the upper limit for F and Y_{n+i} and T_{n+i} are measured and calculated temperatures, respectively, at location x_1 (e.g., the position 2 mm behind the interface in the mold) and at time t. The temperature-time data recorded by the thermocouple near the interface, $Y_1(t)$, were used as the known matching parameters in evaluating the instantaneous heat flux, q_m, while the temperature-time data obtained by the thermocouple farther away from the interface, $Y_2(t)$, were used as timely boundary conditions.

B. Iterative Procedure

The iterative procedure for estimation of the heat flux, which is passing through the mold during solidification, includes the following steps:

(1) Input experimental and thermophysical data.
(2) Set $\varepsilon_1 = 0.001$ incremental value for the heat flux estimation.
(3) Set acceptable convergence criteria coefficients $\varepsilon_2 = 0.005$.
(4) Set the appropriate Fourier number and Δt.
(5) Initialize temperatures with the experimental temperatures.
(6) Guess an initial value for heat flux, q, and calculate appropriate temperatures.
(7) Calculate the sensitivity coefficient.
(8) Calculate the appropriate temperature, T_{n+i}, for the experimental time interval.
(9) Compute the error, $(Y_{n+i} - T_{n+i})$ at the end of the time interval.
(10) Calculate δq^{l+1}.
(11) Check to determine if error satisfies the acceptable convergence criteria $\delta q^{l+1}/q^l \leq \varepsilon_2$. If the criterion is satisfied, then $q^{l+1} = q^l + \delta q^{l+1}$ and continues to process new time interval data by repeating steps 6 through 10. If not, $q^{l+1} = q^l + \delta q^{l+1}$ and steps 7 through 11 are repeated.

The preceding iterative procedure is schematically represented in the flow chart shown in Figure 5.

C. Estimation of the Interfacial Heat-Transfer Coefficient

The heat-transfer coefficient was estimated assuming that a quasi-steady-state condition exists at the casting mold interface.[9,10] The surface temperature in the casting side was estimated from the expression

$$q = -k_{\text{Casting}} \frac{(T_{cs} - T_{Th-3})}{x_{1cs}} \quad [4]$$

where T_{Th-3} is the temperature measured with thermocouple 3 (Figures 1 and 2), x_{1cs} is the distance of thermocouple 3 from the mold surface (2.0 mm), and T_{cs} is the estimated surface temperature of the casting at the mold-casting interface. This temperature was estimated by solving Eq. [4]. Estimations of the temperature of the mold surface and the heat flux at the metal mold
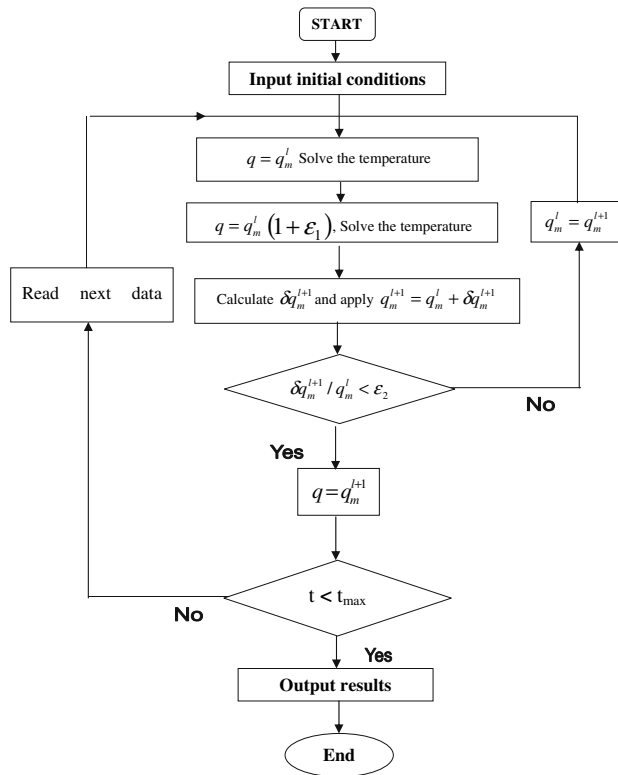

Fig. 4—(a) Display of various boundary conditions in the mold. (b) Mold finite discretization.

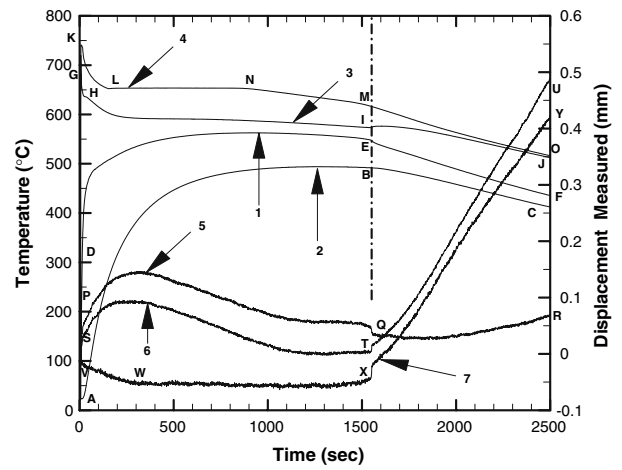Fig. 5—Flow chart for the inverse heat conduction algorithm.

Fig. 6—Typical experimental results obtained. Casting and mold temperature and displacement profiles for steel mold–pure aluminum, steel mold. Surface roughness value $R_a = 1.41$ μm.

interface were computed concurrently. Finally, the heat-transfer coefficient at the casting-mold interface was estimated by the following equation:

$$ h = \frac{q}{(T_{cs} - T_{ms})} \qquad [5] $$

where T_{cs} is the estimated temperature of casting at the casting-mold interface and T_{ms} is the estimated temperature of the mold at the casting-mold interface.

IV. RESULTS AND DISCUSSION

A. Temperature Profiles and Air Gap Development

Figures 6 and 7 provide complementary support in interpreting the data with respect to various aspects of the temperature profiles and air gap development.

Figure 6 shows typical results from a particular experiment involving casting of commercial purity aluminum in a steel mold. The mold's surface roughness value was $R_a \approx 1.41$ μm, and the liquid aluminum had a temperature of 760 °C prior to casting.

Two independent sensors, the LVDTs and thermocouples, detected the onset of the air gap formation and its progressive increase. Lines 5 and 6 depict measurements collected by LVDT-1 and LVDT-2 and represent the relative movements of the mold and casting, respectively. As already mentioned, the difference between the two displacement measurements of the two LVDTs represents the relative movement of the mold-casting metal interface. Line 7 of Figure 6 represents the difference between these two displacement measurements. Examining line 7 further, segment VW represents the period immediately after metal pouring. The negative slope of this segment indicates the expansion of the mold, which is due to the rapid increase in temperature depicted by lines 1 and 2. The rapid increase in temperature occurred in the first 300 seconds of metal solidification. Referring to segment WX of line 7, there was no significant change in the relative position at the mold-casting metal interface. However, there was an abrupt change in the slope of line 7 at point X. This is an indication of the separation at the mold casting metal interface or the onset of the air gap formation. The vertical (dash-dotted) line indicates the time at which the onset of the air gap formation took place. Segment XY of line 7 indicates that the air gap is increasing, which, in turn, provides an additional resistance to the heat flow.
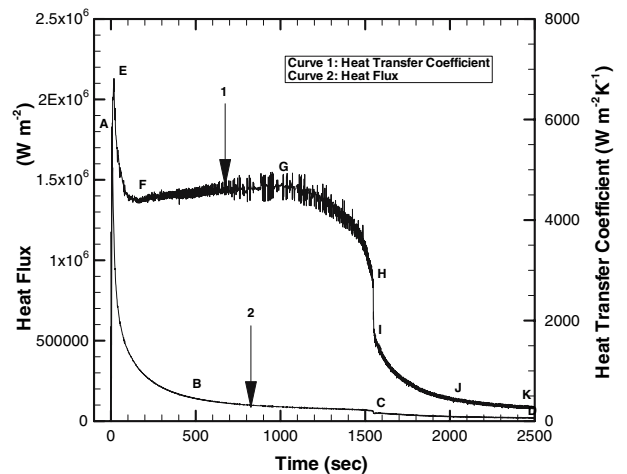

Fig. 7—Inversely estimated parameters for the experimental results shown in Fig. 6.

Lines 1, 2, 3, and 4 represent temperature measurements recorded, respectively, by thermocouples Th-1 and Th-2 (located in the mold) as well as Th-3 and Th-4 (located in the casting). The various segments of these lines indicate different stages in the metal solidification process. The onset of gap formation that was detected by the LVDT displacement measurements described previously was also detected independently by thermocouple measurements. Specifically, segments EF (Line 1) and IJ (Line 3) diverge, indicating the rising thermal resistance due to the fact that the thickness of the air gap is increasing. Consequently, two different types of sensors independently registered the onset of the air gap formation. Through the use of two different sensors, the interpretation made from each could be independently verified. The convergence of the interpretations lent greater validity and increased the assurance that we are, indeed, witnessing the formation of the air gap.

Figure 7 shows the inversely estimated heat-transfer coefficients and heat fluxes associated with the experimental results presented in Figure 6. It is seen from line 1 of Figure 7 that the heat-transfer coefficient reached a maximum (E) in a very short time (18 seconds) following casting. This rise in the heat-transfer coefficient was also associated with the rapid increase in the heat flux (curve 2 in Figure 7). In tandem with that increase, it was noted in Figure 6 that there is a corresponding decrease in the temperature difference between the casting and mold surfaces (Figure 6, lines 1 and 3, from 200 to 1300 seconds). The heat-transfer coefficient depicted in Figure 7, line 1, underwent a rapid decrease (segment EF) once it reached its maximum. This rapid decrease in the heat-transfer coefficient was due to the fact that the rate of heat loss from the casting decreased, as is evident in Figure 6 from the negative slopes of segments GH (curve 3) and KL (curve 4).

In Figure 7, segment FG of line 1 indicates a plateau. The significant expansion of the mold was responsible for this behavior. The following segment, GH, indicates a gradual decrease of the heat-transfer coefficient. This is probably due to the fact that during the time period of segment GH, the solidification front of the metal moved gradually away from the metal mold interface. As such, the grip of the metal to the mold lessened. The gradual decrease of the heat-transfer coefficient in segment GH is followed by an abrupt reduction, denoted by segment HI. This abrupt reduction was due to the onset of the metal mold air gap. At this point, the metal mold separation took place. This interpretation is supported by data in Figure 6, which documented an abrupt change in the metal mold displacement, signified by point X of line 7.

In Figure 7, segment IJK (line 1) denotes a gradual decrease in the heat-transfer coefficient. During this period, the air gap continues to grow. Corroborative evidence for this was provided in Figure 6 by segment XY (line 7). Consequently, as the air gap continued to grow, the corresponding heat-transfer coefficient continued decreasing. Analysis of the data shown in Figure 7 indicates that the heat flux reached a maximum of 1.83×10^6 W m^{-2} within 5 seconds of contact between the liquid metal and the mold. Subsequently,

the heat flux value experienced an exponential decay resulting in an overall average of 1.71×10^3 W m^{-2} by the time separation occurring between the casting and the mold. Within the same time frame, the heat-transfer coefficient value reached a maximum of 6.82×10^3 W m^{-2} K^{-1} within 18.0 seconds before averaging to 4.44×10^3 W m^{-2} K^{-1} at the point of separation.

This experimental work was replicated with the only parameter change being the value of the surface roughness of the steel mold, which was $R_a = 20.72$ μm. Figure 8 displays temperatures and displacements for this case. Figure 9 illustrates the inversely estimated heat-transfer coefficient and heat flux based on the experimental results shown in Figure 8. As such, Figures 8 and 9 depict parallel information as Figures 6 and 7, with the only exception being the value of the mold's surface roughness, which was $R_a = 20.72$ μm instead of the original $R_a = 1.41$ μm. Comparing the results shown in Figures 6 and 8, there is a definite increase in the time of the onset of the air gap formation for Figure 8 (1626 seconds) relative to Figure 6 (1551 seconds). Given that the value of the surface roughness was the sole difference between the two experiments depicted in Figures 6 and 8, the energy removal was faster for the mold with the lower surface roughness value (i.e., $R_a \approx 1.41$ (Figure 6)) than was the case with the higher surface roughness value (i.e., $R_a = 20.72$ μm (Figure 8)). Further comparisons of these two cases yielded additional differences. Figure 9 indicates that the initial maximum heat flux was 1.21×10^6 W/m^2 and the heat-transfer coefficient 3.41×10^3 W/m^2 K reached in 9 and in 13 seconds, respectively. The corresponding values shown in Figure 7 were 1.83×10^6 W m^{-2} and 6.82×10^3 W m^{-2} K^{-1} respectively. Therefore, the value of surface roughness had an impact on both the heat flux and the heat-transfer coefficient. As the value of surface roughness increased, the heat flux and the heat-transfer coefficient decreased.
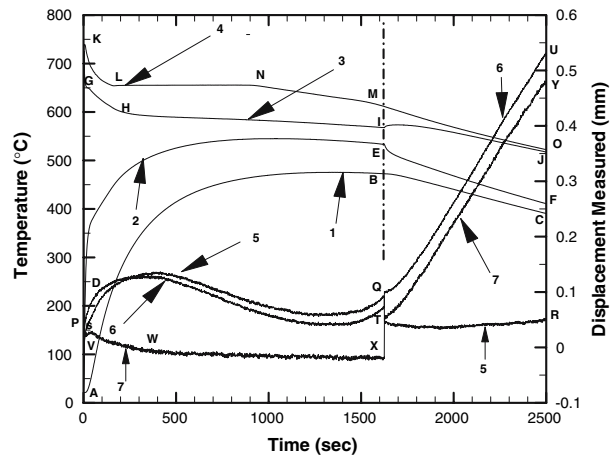

Fig. 8—Typical experimental results obtained. Casting and mold temperature and displacement profiles for steel mold–pure aluminum, steel mold. Surface roughness value $R_a = 20.72$ μm.
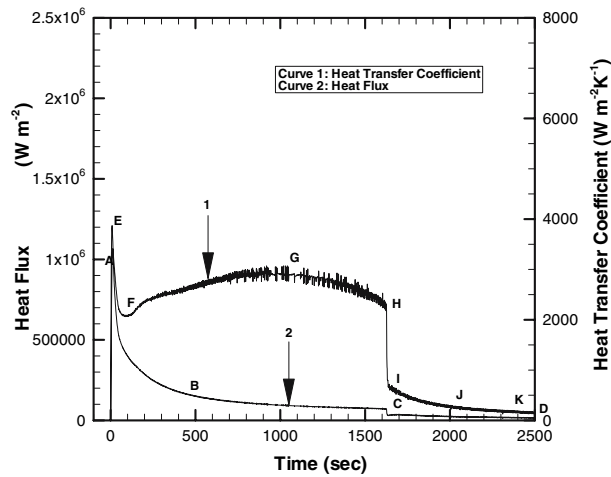
Fig. 9—Inversely estimated parameters for the experimental results shown in Fig. 8.

B. *Effect of Mold Surface Roughness*

Numerous experimental runs were carried out varying mold surface roughness and casting temperature. Three values of surface roughness were used, $R_a = 1.41$ μm, $R_a = 20.72$ μm, and $R_a = 32.69$ μm, and two casting temperatures, 760 °C and 680 °C. The outcomes of the runs at the casting temperature of 760 °C are presented in Figure 10, in the form of inversely estimated heat-transfer coefficients. The corresponding data obtained at the casting temperature of 680 °C are presented in Figure 11.

Examination of Figure 10 indicates that over time comparable trends were evident in the magnitude of the heat-transfer coefficients associated with each of the three values of surface roughness. Beyond this general trend, however, it is clear that during the initial stages of casting, the heat-transfer coefficient was largely affected by the value of the mold's surface roughness. This is evident in segments A1B1C1, A2B2C2, and A3B3C3,
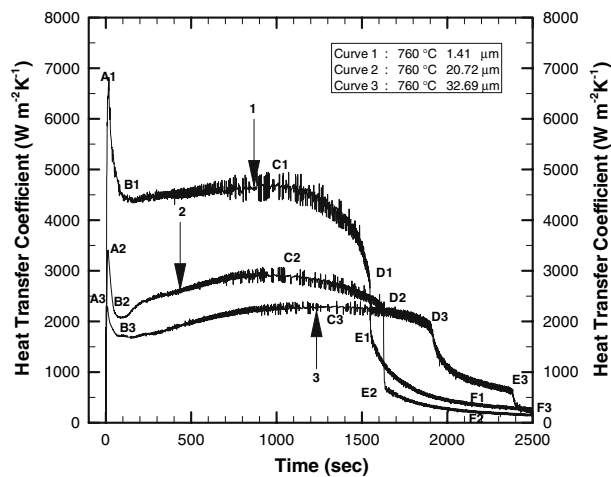
where the highest heat-transfer coefficient corresponded to the lowest value of surface roughness. The local maximum C1, C2, and C3 seemed to occur soon after the arrival of the solidification front at the rear thermocouple denoted by Th-4 in Figure 1. This was anticipated, because at this stage, the contribution of the heat-transfer coefficient by sensible heat cannot be sustained after the major part of the horizontal section of the casting solidified.

Another important feature observed in Figure 10 is that the three curves gradually converge following the metal mold separation (segments E1F1, E2F2, and E3F3). Therefore, once there was a well-developed air gap, the value of the surface roughness had minimal or no effect on the observed heat-transfer coefficient.

Table II summarizes the values of the mold's surface roughness prior to casting, casting conditions, peak, and mean heat-transfer coefficients. Perusal of Table II reveals that mean heat-transfer coefficient values declined as surface roughness values increased, irrespective of the casting temperature. In the case of peak heat-transfer coefficients, however, this relationship with surface roughness values was evident only at the higher casting temperature. (It must be noted that the mean values shown in Table II refer to the time required for the onset of the air gap formation.)

Figure 11 illustrates the effect of surface roughness for the case of 680 °C (20 °C superheat) pouring temperature. Comparing Figure 11 with Figure 10, it is evident that the two figures depict similar relationships. For example, the smaller surface roughness value (curve 1, Figure 11) is associated with higher heat-transfer coefficient values, as shown in Figure 10. Similarly, the curves in Figure 11 gradually converge some time after the metal mold separation, as they did in Figure 10.

The results presented up to this point pertained to a steel mold. It was of interest to determine whether a different metal mold would yield different results. Accordingly, the heat-transfer coefficient and the onset of the air gap formation were studied using a metal mold of high carbon iron. Table I shows some physical characteristics of this mold. Figure 12 presents the heat-transfer coefficients for two surface roughness values, $R_a = 2.34$ μm (line 1) and $R_a = 31.5$ μm (line 2). As seen, the values of the heat-transfer coefficient for

Fig. 10—Estimated heat-transfer coefficients for three different values of surface roughness. Liquid metal temperature: 760 °C. The mold was made from steel.

Table II. Surface Roughness Measurements, Casting Temperatures and Heat-transfer Coefficients for Mold Made From Steel (1020)

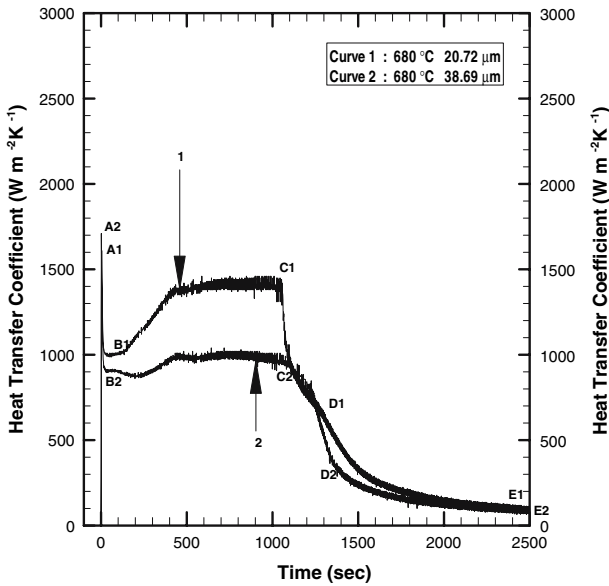| Surface Roughness (R_a)	Casting Temperature °C	Heat-transfer Coefficient (W m^{-2} K^{-1})	
		Peak	Mean
1.41	760	6817	4467
1.41	680	1573	1345
20.72	760	3408	2665
20.72	680	1607	1295
32.69	760	2310	2090
32.69	680	1710	943

Fig. 11—Estimated heat-transfer coefficient for two different values of surface roughness. Liquid metal temperature 680 °C and steel mold.

line 1 are higher than those of line 2, thereby indicating the confirmed inverse relationship between the value of the heat-transfer coefficient and that of surface roughness.

In addition, it was noted that the value of the surface roughness impacted on the time of the onset of the air gap formation. Examination of Figure 12 indicates that the onset of the air gap formation occurs at D1E1 for line 1 ($R_a = 2.34$ μm) and at D2E2 for line 2 ($R_a = 31.5$ μm). As can be seen in Figure 12, segment D1E1 (onset of air gap formation) of line 1 (i.e., lower surface roughness value) occurred earlier than segment

D2E2 of line 2 (i.e., higher surface roughness value). Therefore, the lower surface roughness value was associated with an earlier onset of the air gap formation. This phenomenon was also evident in the case of the steel mold, and moreover, it was apparent at the higher liquid metal temperature of 760 °C (Figure 10) as well as at the lower liquid metal temperature of 680 °C (Figure 11).

Figure 12 depicts an additional characteristic worthy of attention, namely, the convergence of the two curves some time following the air gap formation. This has been evident in all the graphs discussed, regardless of the mold's metal or of the liquid metal temperature. The consistency of this finding lends support to the interpretation provided, namely, that once the air gap forms, the surface roughness value becomes less important to the heat-transfer coefficient.

C. Effect of Casting Metal Superheat

Turning to the secondary aim of this study, namely, the impact of metal temperature on the heat-transfer coefficient, a series of experimental runs were carried out using two different liquid metal temperatures (780 °C and 680 °C) and two mold surface roughness values ($R_a = 20.72$ μm and $R_a = 32.69$ μm).

The effect of the liquid metal superheats on heat-transfer coefficients is depicted in Figure 13 where the value of the surface roughness was $R_a = 20.72$ μm, and in Figure 14 where the surface roughness value was $R_a = 32.69$ μm. Comparisons between the two figures indicated that, regardless of the value of the surface roughness, the higher superheat produced higher heat-transfer coefficients. Also, the inverse relationship between the heat-transfer coefficient and surface roughness that has been demonstrated repeatedly was evident once again. As a result, the highest heat-transfer coefficients were obtained with the higher superheat in conjunction with low surface roughness values.

The effect of superheat on the heat-transfer coefficient may be understood by considering some fundamental
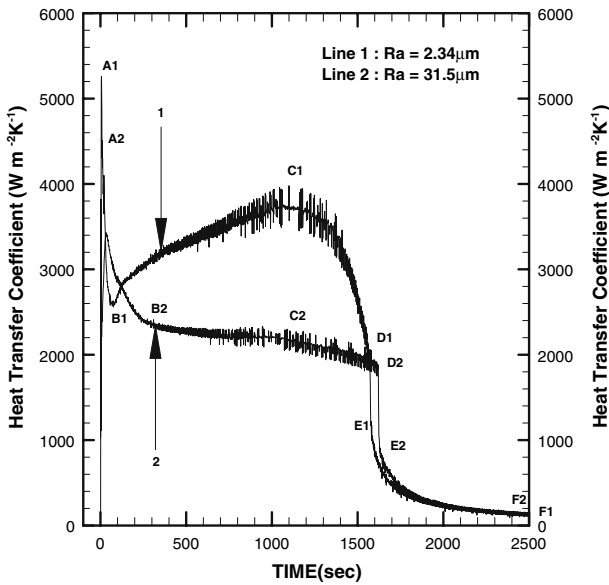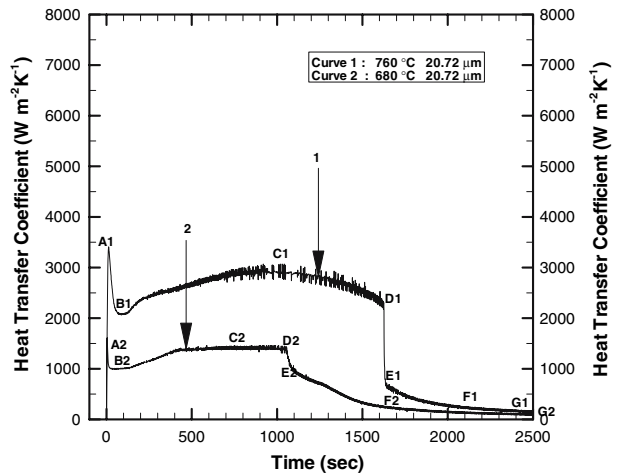

Fig. 12—Estimated heat-transfer coefficients for two different values of surface roughness. Liquid metal temperature: 760 °C. In this case, the metal mold was made from high carbon iron.

Fig. 13—Effect of metal temperature on heat-transfer coefficients. Surface roughness value $R_a = 20.72$ μm steel mold.

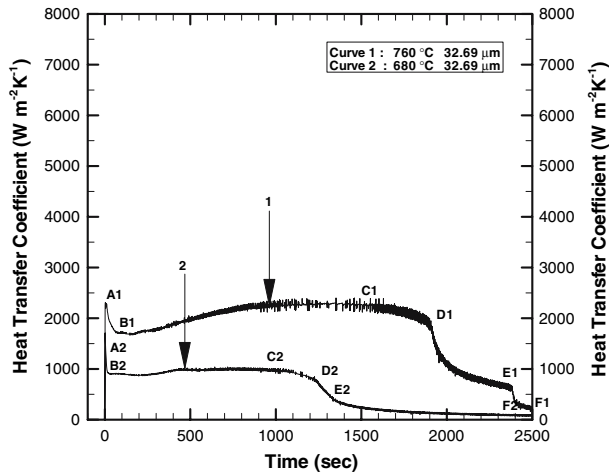Fig. 14—Effect of metal temperature on heat-transfer coefficients. Surface roughness value R_a = 32.69 μm steel mold.
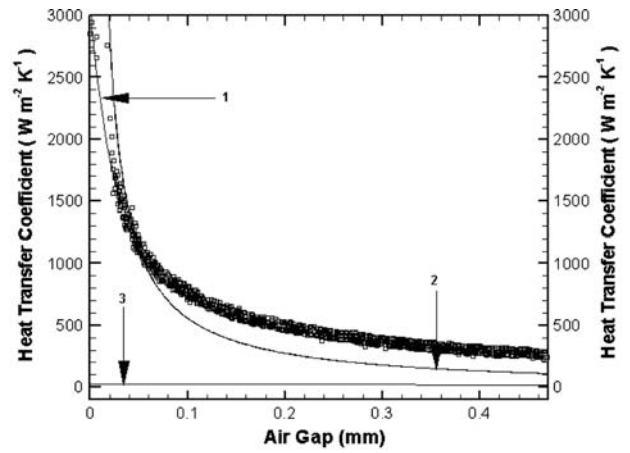

Fig. 15—The squares depict the estimated heat-transfer coefficient and measured air gap size. Line 1 displays predictions based on Eq. [6]. Line 2 shows the theoretical estimations of the heat-transfer coefficient. Line 3 makes visible the estimated radiation heat-transfer coefficient.

concepts of the dynamics of solidification. As liquid metal made initial contact with the peaks of the surface profile, nucleation of the first grains took place. This led to a substantial cooling of the remaining liquid metal, which was in close proximity. As a result, a drop in temperature caused two events to take place simultaneously in the liquid metal. First, the surface tension tended to increase and, second, the fluidity had a tendency to decrease. These two events, coupled with the contraction of the solidified fraction of the liquid metal, hampered the ability of the initial liquid front to penetrate the valley of the rough surface. This phenomenon resulted in reduced contact and, quite naturally, in a reduction in the heat-transfer coefficient at the metal mold interface.

D. *Correlation between the Air-Gap Size and Heat-Transfer Coefficient*

Figure 15 displays estimated heat-transfer coefficient values from the onset of the air gap formation. In this case, estimations of heat-transfer coefficients and measurements of the respective air gap size for the steel mold with surface roughness values of R_a = 1.41 μm were used. A total number of 959 time-steps were correlated. In this correlation, the first time-step corresponded on the onset of air gap formation. The following equation was chosen to correlate the air gap with the respective heat-transfer coefficient:

$$h = \frac{1}{b^*A + c} + d \qquad [6]$$

where

h = heat-transfer coefficient in W m^{-2} K^{-1},
A = air gap size in mm,
b = 1.2318×10^{-2} in W^{-1} m^2 K mm^{-1},
c = 3.3085×10^{-4} in W^{-1} m^2 K, and
d = 116.1491 in W m^{-2} K^{-1}.

The coefficient of multiple determination was computed to be R = 0.991. The air gap size to which Eq. [6] can be applied is $0 \geq A \geq 0.465$ mm.

The squares shown in Figure 15 display the various air gap size and heat-transfer coefficient observations. Line 1 is the graphical representation of Eq. [6]. As seen, Eq. [6] provides an excellent fit for the 959 time-steps. In fact, similar equations were used to correlate air gap size and heat-transfer coefficient involving a cylindrical mold.[4] Line 2 in Figure 15 presents an analytical estimate of the heat-transfer coefficient, assuming a perfectly flat interface between mold-casting metal and temperature varying thermal conductivity of the air.[35] As seen in Figure 15, line 2 tended to underpredict the heat-transfer coefficient when the air gap was larger than 0.05 mm.

Following the onset of the air gap at the metal mold interface, radiation heat transfer may occur in the air gap. In an effort to estimate an effective radiation heat-transfer coefficient, the following equation was used:[4,5]

$$h_{\text{radiation}} = \frac{\sigma \left(T_{cs}^2 + T_{ms}^2 \right) * \left(T_{cs} + T_{ms} \right)}{\frac{1}{\varepsilon_{cs}} + \frac{1}{\varepsilon_{ms}} - 1} \qquad [7]$$

where

σ = Stefan–Boltzmann constant ($= 5.669 \cdot 10^{-8}$ W m^{-2} K^{-4}),
ε_{cs} = emissivity of casting ($= 0.2$), and
ε_{ms} = emissivity of the mold ($= 0.9$).

(Previous equations provide the nomenclature for the other parameters.) Line 3 of Figure 15 depicts the estimated radiation heat-transfer coefficient as a function of the air gap size. It is evident that radiation heat transfer contributed very little to the overall heat-transfer coefficient in the case of aluminum alloy castings. However, in the case of ferrous alloys, it is expected that radiation heat transfer would have a

greater impact due to their higher solidification temperatures. In this respect, similar findings have been reported in References 2 and 6.

The difference between lines 1 and 2 increased as the air gap developed further, which may be attributed to a gradual development of a very small air convection inside the air gap. Conversely, when the air gap has just begun to form, line 2 overpredicted the measured heat-transfer coefficient. A possible explanation for this may be that the very small air convection in the air gap has not yet developed.

V. CONCLUSIONS

A unique and versatile apparatus, instrumented with two types of sensors, was developed to measure the heat-transfer coefficient at the metal mold interface. The concurrent use of two independent sensors provided verification for the collected data. Moreover, the versatility of the apparatus was substantiated by using it with two different metal molds—a steel mold and a high carbon iron mold—and at two different liquid temperatures—780 °C and 680 °C. Finally, the unique apparatus that was developed afforded the opportunity to study the magnitude of the heat-transfer coefficient for an extended period of time following the air gap formation.

Liquid metal temperature was found to influence the estimated values of the heat-transfer coefficient, with higher temperatures producing higher heat-transfer coefficients.

Heat-transfer coefficient values were inversely affected by the value of the surface roughness of the heat extracting mold surface. The onset of the air gap formation was also found to be affected by the value of the surface roughness, with earlier onset associated with lower surface roughness values.

An equation of the form $h = \frac{1}{b*A+c} + d$ was found to provide excellent correlation between the heat-transfer coefficient and air gap size.

ACKNOWLEDGMENT

NOMENCLATURE

A	air gap size (mm)
b	equation constant
c	equation constant
d	equation constant
C_P	specific heat
F	sum-of-squares function
h	heat-transfer coefficient (W/m² K)
k	thermal conductivity (W/m K)
I	upper limit for F
l	iteration step
n	number of temperature measurement
m	time-step number for heat flux vector elements of heat flux at the interface
$\bar{q}$	corresponding to various temperature measurements (W/m²)
R_a	specific surface roughness
T	calculated temperature
T_{cs}	casting surface temperature
T_{ms}	mold surface temperature
Th	thermocouple identification symbol
X	coordinate
Y	measured temperature

GREEK SYMBOLS

ε_1	epsilon, incremental value
ε_2	epsilon, acceptance criterion
ε_{cs}	emissivity of the casting
ε_{ms}	emissivity of the metal mold
α	thermal diffusivity
δ	heat flux increment
ρ	density (kg/m³)
σ	Stefan–Boltzman constant

REFERENCES

1. T.S. Prasanna Kumar and K. Narayan Prabhu: *Metall. Trans. B*, 1991, vol. 22B, pp. 717–29.
2. W.D. Griffiths: *Metall. Mater. Trans. B*, 1999, vol. 30B, pp. 473–82.
3. L.J.D. Sully: *AFS Trans.*, 1976, vol. 84, pp. 735–44.
4. M. Trovant and S. Argyropoulos: *Metall. Mater. Trans. B*, 2000, vol. 31B, pp. 75–86.
5. M. Trovant and S. Argyropoulos: *Metall. Mater. Trans. B*, 2000, vol. 31B, pp. 87–96.
6. Y. Nishida, W. Droste, and S. Engler: *Metall. Trans. B*, 1986, vol. 17B, pp. 833–44.
7. D.G.R. Sharma and M. Krishnan: *AFS Trans.*, 1991, vol. 99, pp. 429–38.
8. C.A. Muojekwu, I.V. Samarasekera, and J.K. Brimacombe: *Metall. Mater. Trans. B*, 1995, vol. 26B, pp. 361–82.
9. K. Ho and R.D. Pehlke: *Metall. Trans. B*, 1985, vol. 16B, pp. 585–94.
10. K. Ho and R.D. Pehlke: *AFS Trans.*, 1984, vol. 92, pp. 587–98.
11. R.D. Pehlke: *Proc. Modelling of Casting, Welding and Advanced Solidification Processes VII*, M. Cross and J. Campbell, eds., TMS, Warrendale, PA, 1995, pp. 373–80.
12. P. Schmidt and I.L. Svensson: *Proc. 7th Int. Conf. Numerical Methods in Thermal Problems*, Vol. VII. I, Pineridge Press Ltd., Swansea, United Kingdom, 1991, pp. 236–47.
13. P. Schmidt: *Mater. Sci. Eng. A*, 1993, vol. A173, pp. 271–74.
14. T.S. Prasanna Kumar and K. Narayan Prabhu: *Metall. Trans. B*, 1991, vol. 22B, pp. 717–29.
15. J. Isaac, G.P. Reddy, and G.K. Sharma: *Br. Foundryman*, 1985, vol. 78, pp. 465–68.
16. M. Krishnan and D.G.R. Sharma: *AFS Trans.*, 1994, vol. 102, pp. 769–74.
17. A.-W.M. Assar: *J. Mater. Sci. Lett.*, 1992, vol. 11, pp. 601–06.
18. M.A. Taha, N.A. El-Mahallawy, A.-W.M. Assar, and R.M. Hammouda: *J. Mater. Sci.*, 1992, vol. 27, pp. 3467–73.
19. M. Krishnan and D.G.R. Sharma: *Scripta Metall. Mater.*, 1993, vol. 28, pp. 447–51.
20. M. Bamberger, B.Z. Weiss, and M.M. Stupel: *Mater. Sci. Technol.*, 1987, vol. 3, pp. 49–56.
21. E. Gozlan and M. Bamberger: *Z. Metallkd.*, 1987, pp. 677–82.

22. N.A. El-Mahallawy and A.M. Assar: *J. Mater. Sci.*, 1991, vol. 26, pp. 1729–33.
23. F. Chiesa: *AFS Trans.*, 1990, vol. 98, pp. 193–200.
24. A.M. Assar: *Mater. Sci. Technol.*, 1977, vol. 13, pp. 702–04.
25. M. Prates and H. Biloni: *Metall. Trans. A*, 1972, vol. 3, pp. 1501–10.
26. B.L. Coates, S.A. Argyropoulos, and B. Melissari: *Proc. Int. Symp. on Enabling Technologies for Light Metals and Composite Materials and Their End-Products*, TMS-CIM, 2002, pp. 487–501.
27. T. Loulou, E.A. Artyukhin, and J.P. Bardon: *Int. J. Heat Mass Transfer*, 1999, vol. 42, pp. 2119–27.
28. T. Loulou, E.A. Artyukhin, and J.P. Bardon: *Int. J. Heat Mass Transfer*, 1999, vol. 42, pp. 2129–42.
29. G.X. Wang and E.F. Matthys: *Int. J. Heat Mass Transfer*, 2002, vol. 45, pp. 4967–81.
30. W. Wang and H.H. Qiu: *Int. J. Heat Mass Transfer*, 2002, vol. 45, pp. 2043–53.
31. A. Venkatesan, K. Suchithra, and A. Rajadurai: *AFS Trans.*, 2005, vol. 113, in CD format, paper 05-069(02).pdf.
32. R. Kayikci, W.D. Griffiths, and C. Strangeways: *J. Mater. Sci.*, 2003, vol. 38, pp. 3683–87.
33. J.V. Beck: *Int. J. Heat Mass Transfer*, 1970, vol. 13, pp. 703–16.
34. Serope Kalpakjian and Steven R. Schmid: *Manufacturing Engineering and Technology*, Vol. 4, Prentice Hall, Elmsford, NJ, 2000, pp. 272.
35. F.P. Incropera and D.P. Dewitt: *Fundamentals of Heat and Mass Transfer*, 3rd ed., John Wiley & Sons, New York, NY, 1990, Appendix A, p. A15.